# A Silicon Monolithic Phase-Inverter Rat-Race Coupler Using Spiral Coplanar Striplines and Its Application in a Broadband Gilbert Mixer

Sheng-Che Tseng, *Student Member, IEEE*, Chinchun Meng, *Member, IEEE*, Chia-Hung Chang, Shih-Hsien Chang, and Guo-Wei Huang

***Abstract*—This paper realized a broadband uniplanar phase-inverter rat-race coupler using a standard silicon process, and then analyzed this coupler under a lossy condition. A phase inverter is employed in this coupler, not only to extend the operation bandwidth, but also to generate balanced outputs by providing equal lossy paths, while symmetrical spiral-shaped coplanar striplines (CPSs) are also utilized to shrink the coupler size, as well as to construct a phase inverter in the middle of one of spiral CPSs. The lossy CPS, when designed as a distortionless line, has a real characteristic impedance, and thus, perfect port matching of the coupler can be achieved at the center frequency. The operation frequency of this silicon monolithic rat-race coupler with the size of 0.5 mm$^2$ is extremely wide and ranges from 5 to 23 GHz. The dissipated loss, transmission coefficient, and isolation of the rat-race coupler are approximately 5.5, −8, and below −25 dB, respectively. In addition, a wideband Gilbert micromixer with an integrated uniplanar phase-inverter rat-race coupler at the local oscillator port is demonstrated using 0.35-$\mu$m SiGe BiCMOS technology. This mixer works from 2.5 to 13 GHz with 12-dB conversion gain, −16-dBm $IP_{1\,dB}$, −4-dBm $IIP_3$, and 14-dB noise figure. The chip size of the mixer with an integrated coupler is approximately 1.4 mm × 1.4 mm.**

***Index Terms*—Downconverter, micromixer, phase inverter, rat-race coupler, SiGe BiCMOS, silicon substrate, transimpedance amplifier, wideband.**

## I. Introduction

SILICON-BASED technologies have the properties of high integration and low-cost production. Active devices have advanced in possession of the cutoff frequency of more than 100 GHz, and they are suitable for microwave and millimeter-wave applications [1]. Today, passive components are largely implemented using silicon-based technologies in RF integrated circuits (ICs). For example, inductors and transformers are applied in oscillators, low-noise amplifiers, and mixers [2]. However, the standard silicon substrate with a resistivity of approximately 10 $\Omega \cdot$ cm deteriorates signals, causes crosstalk between two adjacent passives, and influences the functions of passive components. Thus, it is a big challenge to form useful RF passive components on a silicon substrate for microwave and millimeter-wave applications [3], [4].

To reduce the substrate loss, many solutions have been developed, such as micromachining, high-resistivity substrate, silicon-on-insulator (SOI) process, and shielding. Abidi *et al.* applied the front-side micromachining to form a suspended inductor in a CMOS RF amplifier. Thus, this inductor has higher self-resonance frequency and quality factors and can work at higher frequencies [5]. The backside micromachining is also employed to eliminate the unpredictable pattern-dependent etching behavior of front-side micromachining [6], [7]. Besides this, the high-resistivity ($\sim$ 1 k$\Omega \cdot$ cm) silicon substrate is also employed, but the entire substrate with high resistivity is not compatible with active devices, due to the latch-up issue [8]. The local high-resistivity substrate can be obtained by proton-damaged ion implantation with high energy (15 MeV) before the backend process, or with low energy ($\sim$4 MeV) after the backend process [9]. The substrate resistivity increases significantly to $\sim$ 1 M$\Omega \cdot$ cm. The performances of the transmission lines and spiral inductors on the proton-damaged high-resistivity silicon substrate are enhanced [9], [10]. Shielding, like patterned ground shields [11] and floating shields [4], is inserted between the signal path and the silicon substrate, to resist the substrate loss without any extra process. This method is adequate for the process with multiple metal layers.

A rat-race coupler is a commonly used four-port passive component, with three one-quarter-wavelength and one three-quarter-wavelength transmission lines. The three-quarter-wavelength segment offers a 180° phase delay to generate differential signals at the neighboring ports and to cancel signal at the opposite isolation port. These properties are achieved at a specified frequency, and thus, the bandwidth is limited. In the case of the uniplanar transmission line, there exists an effective way to minimize the size and to extend the bandwidth simultaneously for the rat-race coupler. A phase inverter is employed in the middle of the quarter-wavelength transmission line to replace the three-quarter-wavelength section, as shown in Fig. 1(a) [12]–[16]. On account of the wideband and low-loss properties of the phase inverter, the operation bandwidth of a phase-inverter rat-race coupler is

Manuscript received January 22, 2008; revised May 26, 2008. First published July 15, 2008; last published August 8, 2008 (projected). This work was supported by the National Science Council of Taiwan, R.O.C., under Contract NSC 96-2752-E-009-001-PAE and Contract NSC 95-2221-E-009-043-MY3, by the Ministry of Economic Affairs of Taiwan under Contract 96-EC-17-A-05-S1-020, by the Ministry of Education (MOE) Aiming for the Top University and Elite Research Center Development (ATU) Plan under Contract 95W803, and by the National Chip Implementation Center (CIC).

S.-C. Tseng, C. Meng, C.-H. Chang and S.-H. Chang are with the Department of Communication Engineering, National Chiao Tung University, Hsinchu 300, Taiwan, R.O.C. (e-mail: shengche.cm92g@nctu.edu.tw; ccmeng@mail.nctu.edu.tw; s891206@hotmail.com; jacky.chang@sunplus.com).

G.-W. Huang is with National Nano Device Laboratories, Hsinchu 300, Taiwan, R.O.C. (e-mail: gwhuang@mail.ndl.org.tw).

Color versions of one or more of the figures in this paper are available online at http://ieeexplore.ieee.org.

Digital Object Identifier 10.1109/TMTT.2008.927312

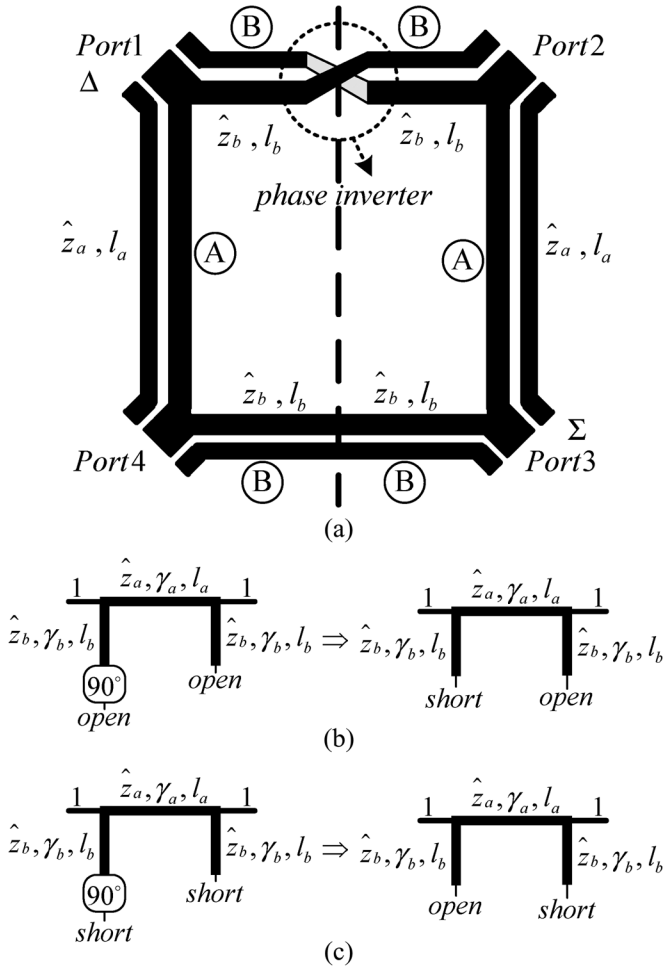


Fig. 1. Even- and odd-mode analyses of a phase-inverter rat-race coupler. (a) Phase-inverter rat-race coupler. (b) Even mode of the phase-inverter rat-race coupler. (c) Odd mode of the phase-inverter rat-race coupler.

very large. This rat-race coupler maintains balanced output signals regardless of the substrate loss, thanks to the equal path loss. Couplers had been realized on the silicon substrate, but most of them are created with substrate shielding [17], [18], which results in a low effective dielectric constant, and thus, a large coupler size. It is advantageous to implement the coupler directly on the silicon substrate for size reduction by the higher effective dielectric constant. The finite-ground coplanar waveguide (FGCPW) phase-inverter rat-race couplers directly on the silicon substrate had been implemented at 60 and 77 GHz [19], and size-reduction techniques were applied at the cost of the bandwidth even at such high frequencies [15].

In this paper, the balanced structure of passive components is analyzed and designed to mitigate the influence of the substrate loss by means of using two signal paths with equal loss. This research focuses on a uniplanar transmission line rat-race coupler implemented directly on lossy silicon substrate. Here, the uniplanar transmission lines—coplanar waveguides (CPWs) and coplanar striplines (CPSs)—demand few metal layers and have the higher effective dielectric constant for size reduction when compared with microstrip lines formed by the inter-metal dielectric, sandwiched by the top metal and bottom shielding ground metal [17], [18], [20]. In addition, spiral-shaped CPSs are also employed to shrink the size. A phase-inverter rat-race coupler using symmetrical spiral CPSs is implemented directly on a low-resistivity ($\sim 10\ \Omega \cdot$ cm) standard silicon substrate in this paper. The phase inverter in the rat-race coupler is the key element to keep outputs balanced by providing the equal-length lossy paths, and thus, the phase-inverter rat-race coupler preserves the broadband properties even in the presence of lossy silicon substrate. In addition, the lossy CPS is designed as a distortionless transmission line to have a nondispersive and real characteristic impedance for broad bandwidth and perfect port matching of the coupler. This paper also demonstrated a wideband Gilbert mixer with this integrated coupler using a 0.35-$\mu$m SiGe BiCMOS process. The integrated wideband phase-inverter rat-race coupler can eliminate the problem of poor differential signals caused by the mismatch of the external balun and cables.

## II. Circuit Design

In this paper, a spiral-shaped CPS is applied for size reduction to the phase-inverter rat-race coupler directly on the standard silicon substrate at a low-frequency regime without any compromise in the bandwidth. Moreover, the phase-inverter rat-race coupler is analyzed under the lossy condition and a distortionless transmission-line design methodology is developed for the simple port-matching condition. Many previous analyses have focused on a lossless rat-race coupler [15]. Here, the even- and odd-mode analyses are applied to analyze a lossy rat-race coupler with a phase inverter, as shown in Fig. 1 [21]. Ports 1 and 3 are the delta and sum ports, respectively. The length and complex propagation constant of the transmission lines, A and B, in Fig. 1(a) are denoted as $l_a$, $\gamma_a$, $l_b$, and $\gamma_b$, respectively. The normalized characteristic impedances $\hat{z}_a$ and $\hat{z}_b$ of the transmission lines, with respect to the terminal impedance $Z_0$ are, in general, complex, as described in [22]. The even-mode network consists of a transmission line with one short shunt stub and one open shunt stub on two sides and this network becomes the odd-mode network by exchanging two shunt stubs, as shown in Fig. 1(b) and (c). The even- and odd-mode $ABCD$ matrices are then derived as

$$\begin{aligned}\begin{bmatrix} A & B \\ C & D \end{bmatrix}_e &= \begin{bmatrix} 1 & 0 \\ \dfrac{1}{\hat{z}_b}\coth(\gamma_b \ell_b) & 1 \end{bmatrix} \\ &\quad \times \begin{bmatrix} \cosh(\gamma_a \ell_a) & \hat{z}_a \sinh(\gamma_a \ell_a) \\ \dfrac{1}{\hat{z}_a}\sinh(\gamma_a \ell_a) & \cosh(\gamma_a \ell_a) \end{bmatrix} \\ &\quad \times \begin{bmatrix} 1 & 0 \\ \dfrac{1}{\hat{z}_b}\tanh(\gamma_b \ell_b) & 1 \end{bmatrix} \\ &= \begin{bmatrix} a & b \\ c & d \end{bmatrix} \end{aligned} \tag{1}$$

and

$$\begin{aligned}\begin{bmatrix} A & B \\ C & D \end{bmatrix}_o &= \begin{bmatrix} 1 & 0 \\ \dfrac{1}{\hat{z}_b}\tanh(\gamma_b \ell_b) & 1 \end{bmatrix} \\ &\quad \times \begin{bmatrix} \cosh(\gamma_a \ell_a) & \hat{z}_a \sinh(\gamma_a \ell_a) \\ \dfrac{1}{\hat{z}_a}\sinh(\gamma_a \ell_a) & \cosh(\gamma_a \ell_a) \end{bmatrix} \\ &\quad \times \begin{bmatrix} 1 & 0 \\ \dfrac{1}{\hat{z}_b}\coth(\gamma_b \ell_b) & 1 \end{bmatrix} \\ &= \begin{bmatrix} d & b \\ c & a \end{bmatrix} \end{aligned} \tag{2}$$

respectively, where

$$\begin{aligned} a &= \cosh(\gamma_a \ell_a) + \frac{\hat{z}_a}{\hat{z}_b}\tanh(\gamma_b \ell_b)\sinh(\gamma_a \ell_a) \\ b &= \hat{z}_a \sinh(\gamma_a \ell_a) \\ c &= \frac{1}{\hat{z}_b}\cosh(\gamma_a \ell_a)\left[\tanh(\gamma_b \ell_b) + \coth(\gamma_b \ell_b)\right] \\ &\quad + \sinh(\gamma_a \ell_a)\left[\frac{1}{\hat{z}_a} + \frac{\hat{z}_a}{\hat{z}_b^2}\right] \\ d &= \cosh(\gamma_a \ell_a) + \frac{\hat{z}_a}{\hat{z}_b}\coth(\gamma_b \ell_b)\sinh(\gamma_a \ell_a). \end{aligned} \tag{3}$$

Deriving from the even- and odd-mode $ABCD$ matrices, the $S$-parameter matrix of the phase-inverter rat-race coupler can be written as

$$\begin{aligned} [S] &= \frac{1}{a+b+c+d}\begin{bmatrix} b-c & a-d & 0 & 2 \\ a-d & b-c & 2 & 0 \\ 0 & 2 & b-c & d-a \\ 2 & 0 & d-a & b-c \end{bmatrix} \\ &= \begin{bmatrix} S_{11} & S_{21} & S_{31} & S_{41} \\ S_{21} & S_{11} & S_{41} & S_{31} \\ S_{31} & S_{41} & S_{11} & -S_{21} \\ S_{41} & S_{31} & -S_{21} & S_{11} \end{bmatrix} \end{aligned} \tag{4}$$

where $S_{11}$, $S_{21}$, $S_{31}$, and $S_{41}$ are expressed in (5), shown at the bottom of this page.

Under the design conditions that $l_a = 2l_b = l$, $\hat{z}_a = \hat{z}_b = \hat{z}$, and $\gamma_a = \gamma_b = \alpha + j\beta$, $S_{21}$ is equal to $-S_{41}$ no matter what the operation frequency is, as is derived from Appendix A. Obviously, the phase inverter is properly employed to keep the signal lossy paths equal so that the differential outputs of the coupler maintain balance in magnitude and phase. In the case of no loss, the $S$-parameters are the same as the $S$-parameters derived in [15].

According to the derivation shown in Appendix B, the perfect port-matching is achieved at the center frequency with the wavelength $l = \lambda/4$ when the normalized characteristic impedance of the rat-race coupler is equal to

$$\hat{z} = \frac{\sqrt{2\cosh\left(\dfrac{\lambda\alpha}{2}\right)}}{\cosh\left(\dfrac{\lambda\alpha}{4}\right)}. \tag{6}$$

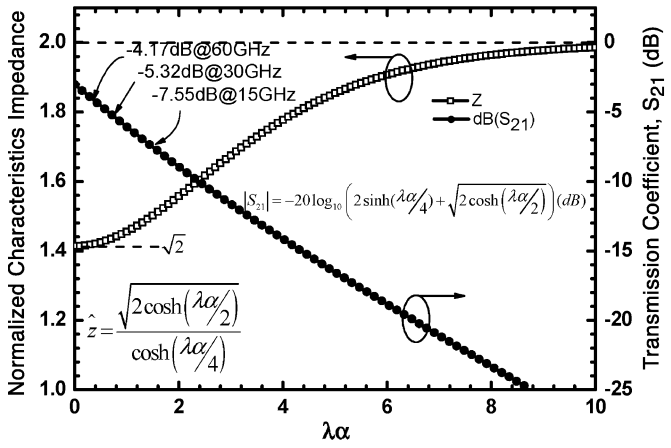


Fig. 2. Normalized characteristic impedance and transmission coefficient with respect to $\lambda\alpha$ for perfect matching.

The normalized characteristic impedance $\hat{z}$ is a function of $\lambda\alpha$, and the minimum and maximum values are $\sqrt{2}$ and 2, respectively. Fig. 2 reveals that the characteristic impedance for perfect matching is always a real number, which occurs only under the lossless or distortionless conditions [23]. Therefore, the transmission line is designed as a near distortionless line in our study to achieve perfect matching. Theoretically, $S_{21}$ is equal to $-S_{41}$. The bandwidth of the coupler is limited by the matching condition. In order to extend the bandwidth, the perfect port matching could be designed at more frequencies around the center frequency, as mentioned in [16]. Nevertheless, the lossy coupler has broader input matching than the lossless counterpart because of the degradation of the quality factor of the transmission line. In our study, the rat-race coupler is directly implemented on a lossy substrate for a compact size, and the dielectric loss is dominant. The loss is proportional to the length of the transmission line. For high-frequency applications, a shorter transmission line length reduces loss. As is derived from Appendix B, the transmission coefficient $S_{21}$, at the center frequency, can be expressed in terms of $\lambda\alpha$

$$|S_{21}| = -20\log_{10}\left(2\sinh\left(\frac{\lambda\alpha}{4}\right) + \sqrt{2\cosh\left(\frac{\lambda\alpha}{2}\right)}\right)\ (\text{dB}). \tag{7}$$

As shown in Fig. 2, with the same attenuation constant, $\alpha = 2.1\ \text{cm}^{-1}$, the transmission coefficient $S_{21}$ becomes $-7.55$, $-5.32$, and $-4.17$ dB, at the operation frequency of 15,

$$\begin{aligned} S_{11} &= \frac{\sinh(\gamma_a \ell_a)\left(\hat{z}_a - 1/\hat{z}_a - \hat{z}_a/\hat{z}_b^2\right) - 1/\hat{z}_b\cosh(\gamma_a \ell_a)\left[\tanh(\gamma_b \ell_b) + \coth(\gamma_b \ell_b)\right]}{2\cosh(\gamma_a \ell_a) + 1/\hat{z}_b\left[\hat{z}_a\sinh(\gamma_a \ell_a) + \cosh(\gamma_a \ell_a)\right]\left[\tanh(\gamma_b \ell_b) + \coth(\gamma_b \ell_b)\right] + \sinh(\gamma_a \ell_a)\left[\hat{z}_a + 1/\hat{z}_a + \hat{z}_a/\hat{z}_b^2\right]} \\ S_{21} &= \frac{\dfrac{\hat{z}_a}{\hat{z}_b}\sinh(\gamma_a \ell_a)\left[\tanh(\gamma_b \ell_b) - \coth(\gamma_b \ell_b)\right]}{2\cosh(\gamma_a \ell_a) + 1/\hat{z}_b\left[\hat{z}_a\sinh(\gamma_a \ell_a) + \cosh(\gamma_a \ell_a)\right]\left[\tanh(\gamma_b \ell_b) + \coth(\gamma_b \ell_b)\right] + \sinh(\gamma_a \ell_a)\left[\hat{z}_a + 1/\hat{z}_a + \hat{z}_a/\hat{z}_b^2\right]} \\ S_{31} &= 0 \\ S_{41} &= \frac{2}{2\cosh(\gamma_a \ell_a) + 1/\hat{z}_b\left[\hat{z}_a\sinh(\gamma_a \ell_a) + \cosh(\gamma_a \ell_a)\right]\left[\tanh(\gamma_b \ell_b) + \coth(\gamma_b \ell_b)\right] + \sinh(\gamma_a \ell_a)\left[\hat{z}_a + 1/\hat{z}_a + \hat{z}_a/\hat{z}_b^2\right]} \end{aligned} \tag{5}$$

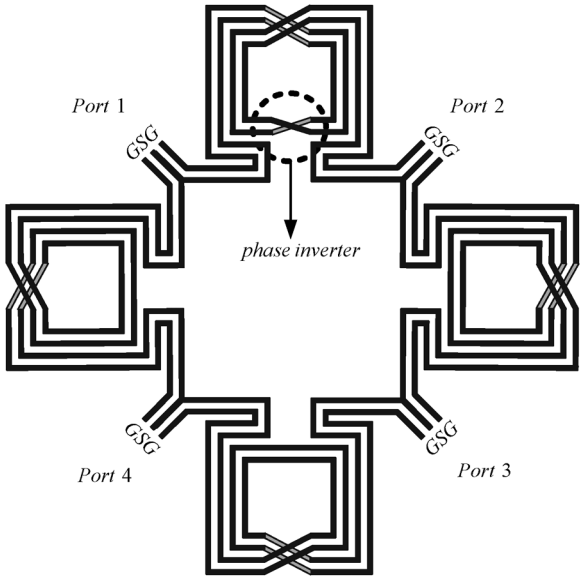


Fig. 3. Symmetrical spiral-shaped CPS rat-race coupler with a phase inverter.

30, and 60 GHz, respectively. This loss at 60 GHz is consistent with [19]. Our proposed rat-race coupler directly on a low-resistivity substrate is more suitable at higher frequencies. A lumped-element technique is also useful to shorten the length and then to lessen the loss at the cost of the operation bandwidth. Though a high coupler loss occurs for low-frequency applications, the coupler is useful to provide wideband differential signals to the local oscillator (LO) port of a Gilbert mixer. This is because the differential pair of the bipolar/MOS Gilbert cell needs a small twist voltage to commutate an RF current. However, the lossy coupler is not appropriate for diode mixers, which demand large LO pumping power. Besides, the coupler is not useful to be employed in the RF port of a downconverter because the high coupler loss results in a high noise figure.

Fig. 3 shows the layout of the phase-inverter CPS rat-race coupler. Quarter-wavelength CPSs are winding into a symmetrical spiral shape to condense the estate of the coupler. In addition, the phase inverter is easily established in the middle of the symmetrical spiral-shaped CPSs to provide a 180° phase shift, as shown in Fig. 3. The physical size of the phase inverter should be negligible when compared with the operating wavelength. The transmission line can be modeled in terms of the per-unit-length resistance $\widetilde{R}$, inductance $\widetilde{L}$, conductance $\widetilde{G}$, and capacitance $\widetilde{C}$ [23]. The transmission-line parameters are extracted from the electromagnetic (EM)-simulated $S$-parameters [24]. For a fixed CPS gap, $\widetilde{R}$ decreases with the CPS width increase, so that the distortionless condition is achieved by controlling the metal width. The characteristic impedance for the matching condition varies smoothly from $\sqrt{2}\ Z_0$ to $2Z_0$. Thus, the transmission-line impedance approaches the characteristic impedance for the matching condition of a proper CPS gap. With this systematic design, the input matching and distortionless property are achieved approximately at the same time. Wave propagates well in straight CPSs. However, coupling occurs at the bends of the spiral-shaped lines. The spacing between adjacent CPSs is a tradeoff between layout size and coupling. The optimal spacing between adjacent CPSs from the simulations is close to the CPS line-to-line spacing. Moreover, the bends in the spiral-shaped CPSs are a small proportion of entire quarter-wavelength transmission lines, and hence, the change of impedance or transmission-line parameters of this section can be neglected from the EM simulations.

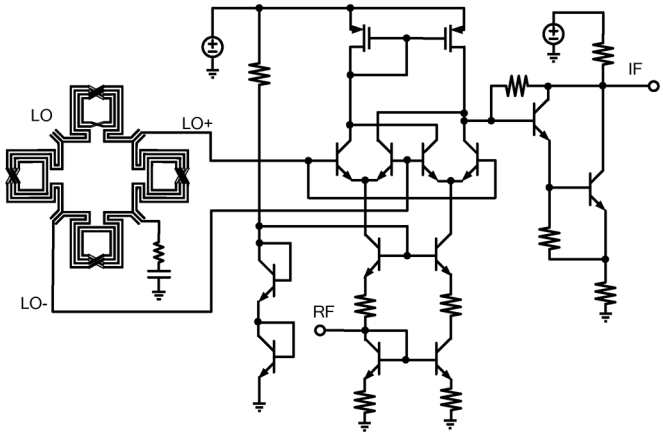


Fig. 4. Schematic of the micromixer with a phase-inverter rat-race coupler.

In our complete analysis, the lossy rat-race coupler with a phase inverter has wideband operation and still keeps outputs balanced because of equal path loss. It is interesting that a distortionless line is employed to achieve a simple port-matching condition. The matching condition and bandwidth performance are different from those under the lossless condition analysis [15]. The shorter a transmission line is, the smaller the loss is. Therefore, the lossy phase-inverter rat-race coupler is suitable for high frequencies because of the compact size as well as the small loss.

The schematic of the entire mixer with an LO phase-inverter rat-race coupler is shown in Fig. 4. A micromixer employed in this paper [25] is the same as the micromixer presented in our previous study, and more details about the micromixer design are described in our previous publication [22].

## III. Measurement Results

### A. Micromixer With an Integrated Phase-Inverter Rat-Race Coupler

The micromixer with an integrated phase-inverter rat-race coupler is fabricated using 0.35-$\mu$m SiGe BiCMOS technology with three metal layers. The die photograph is displayed in Fig. 5 and the active circuitry is inside the rat-race coupler for a compact layout. The chip size is approximately 1.4 mm × 1.4 mm. The transistors of the mixer core are SiGe HBT devices with a peak cutoff frequency of 67 GHz, while the rat-race coupler is mainly formed by the top metal. The total current consumption is approximately 32 mA at the supply voltage of 5 V. Fig. 6 presents the wideband performance of this micromixer. Thanks to the RF wideband matching and LO broadband phase-inverter rat-race coupler, this mixer works with a 3-dB bandwidth of 10.5 GHz from 2.5 to 13 GHz. The conversion gain is approximately 12 dB. The mixer needs only 0-dBm LO power to function after taking the dissipated loss of the coupler into consideration because the SiGe HBT transistors in the Gilbert cell switching quad only need small power to perform the current commutation. Fig. 6 also exhibits that the input 1-dB gain compression point $\mathrm{IP}_{1\,\mathrm{dB}}$ and the input third-order intercept

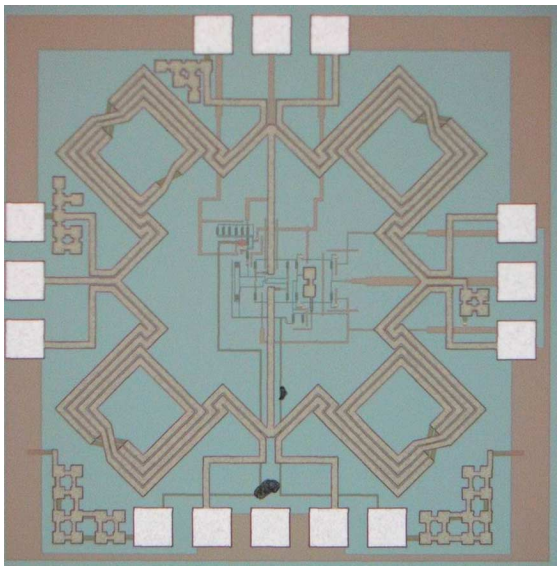

Fig. 5. Die photograph of the micromixer with an integrated phase-inverter rat-race coupler.

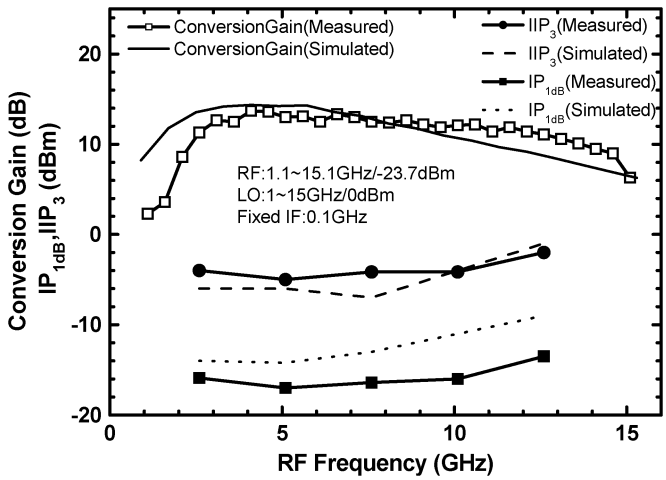


Fig. 6. Conversion gain $\mathrm{IP}_{1\ \mathrm{dB}}$ and $\mathrm{IIP}_3$ of the micromixer with an integrated phase-inverter rat-race coupler.

point $\mathrm{IIP}_3$ are approximately $-16$ and $-4$ dBm, respectively. The power performance is measured at 2.6, 5.1, 7.6, 10.1, and 12.6 GHz.

The noise figure of the micromixer with an integrated phase-inverter rat-race coupler is measured at fixed LO frequencies of 5, 7, and 9 GHz. The minimum noise figure is approximately 14 dB, as shown in Fig. 7. The noise figure does not vary very much with LO frequency. As shown in Fig. 8, the 3-dB bandwidth is approximately 400 MHz. The LO-to-IF and LO-to-RF isolations are below $-30$ dB, while the RF-to-IF isolation is below $-25$ dB. The input return loss at the RF and LO ports and the output return loss at the IF port are measured. Since the RF-input stage is a micromixer with a wideband matching property, and the IF-output stage utilizes a Darlington pair of transistors along with a resistive feedback technique, the return loss at the RF and IF ports is below $-10$ dB. The perfect LO-input matching occurs at 7 GHz. The simulations are performed by the post-layout extraction of active circuits, as well as by the

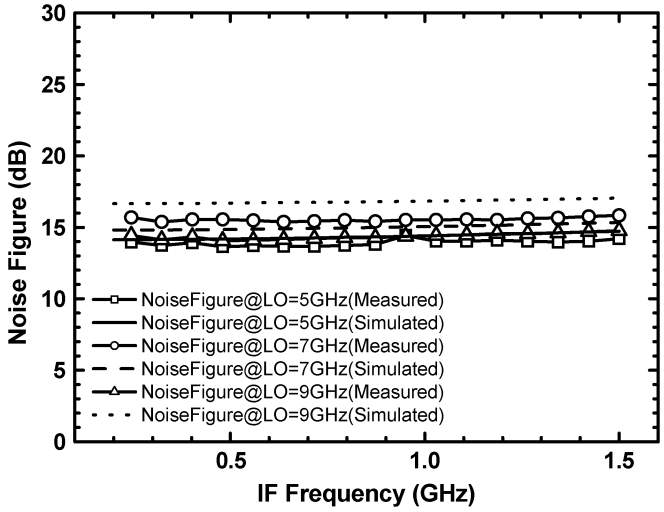


Fig. 7. Noise figure of the micromixer with an integrated phase-inverter rat-race coupler.

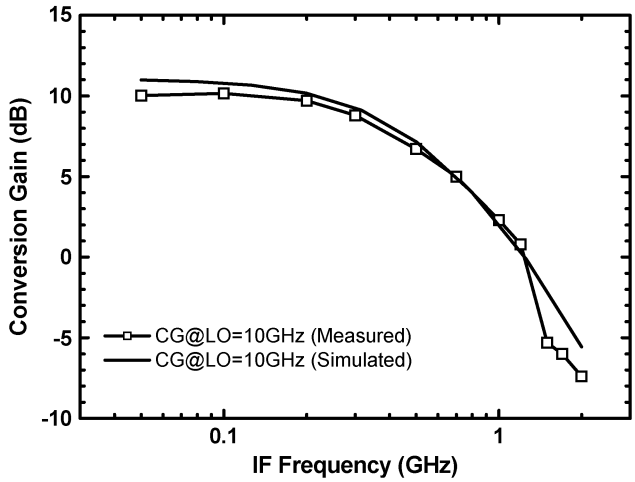


Fig. 8. Conversion gain of the micromixer with an integrated phase-inverter rat-race coupler with respect to IF frequencies.

EM simulation of the rat-race coupler. The measurements are close to the simulations.

### *B. Symmetrical Spiral-Shaped Phase-Inverter Rat-Race Coupler*

A symmetrical spiral-shaped rat-race coupler with a phase inverter was implemented on a low-resistivity ($\sim 10\ \Omega \cdot$ cm) silicon substrate. A die photograph is shown in Fig. 9, and the chip estate, including pads, is $1 \times 1$ mm$^2$. However, the coupler size is only 0.5 mm$^2$, while each spiral-shaped CPS takes on an area of 250 $\mu$m $\times$ 250 $\mu$m. In addition, circuitry, like a mixer, can be arranged in the center of the rat-race coupler to save the area without performance degradation, as shown in Fig. 5. The rat-race coupler here is designed at the center frequency of 14.5 GHz, while the rat-race coupler employed in the mixer is designed at the center frequency of 7.7 GHz. The phase-inverter rat-race coupler is formed by the top two metals with a thickness of 0.925 and 0.64 $\mu$m. The width, spacing, and length of the quarter-wavelength CPS are 15, 5, and approximately 1800 $\mu$m, respectively. The measurement is performed by a four-port network analyzer with on-wafer probes on four sides of the die.

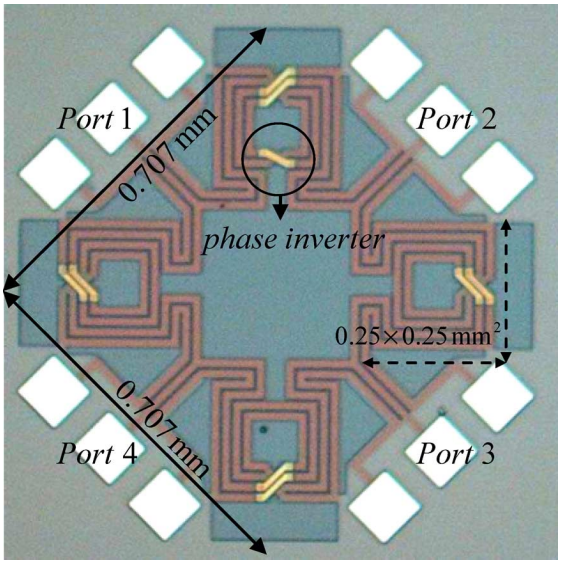


Fig. 9. Die photograph of the rat-race coupler with a phase inverter.

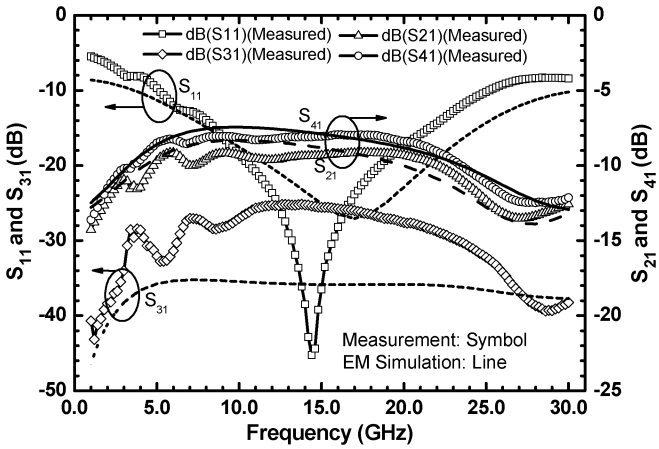


Fig. 10. $S$-parameters of the rat-race coupler with a phase inverter.

Ports 1 and 3 are the delta and sum ports, respectively. Fig. 10 shows the magnitude of $S_{11}$, $S_{21}$, $S_{31}$, and $S_{41}$ from the measurement and the IE3D EM simulation. This phase-inverter rat-race coupler functions from 5 to 23 GHz with a 4.6-to-1 bandwidth ratio. The bends in the spiral-shaped CPSs, in the IC process, are a small proportion of the entire transmission lines. Thus, the bandwidth of the phase-inverter rat-race coupler implemented by IC technology is comparable with that implemented on the printed circuit board [14], [15]. There is perfect port-matching at 14.5 GHz, and the isolation between the delta and sum ports ($S_{31}$) is below $-25$ dB. The magnitude imbalance between $S_{21}$ and $S_{41}$ is small and approximately 1 dB, as shown in Fig. 11, resulting from the phase inverter. However, the phase difference is always close to 180°. The maximum phase and magnitude errors are 8.5° and 1.6 dB within the operation frequencies of 5–23 GHz, respectively. The performance of the signals, when fed from the sum port, is displayed in Fig. 12. The phase difference stays at around 0° and the difference in magnitude is close to 0 dB. The dissipated loss of the phase-inverter rat-race coupler is defined as

$$\text{Loss} = -10\log\left(|S_{11}|^2 + |S_{21}|^2 + |S_{31}|^2 + |S_{41}|^2\right) \quad (8)$$

and is approximately 5.5 dB, as shown in Fig. 13.

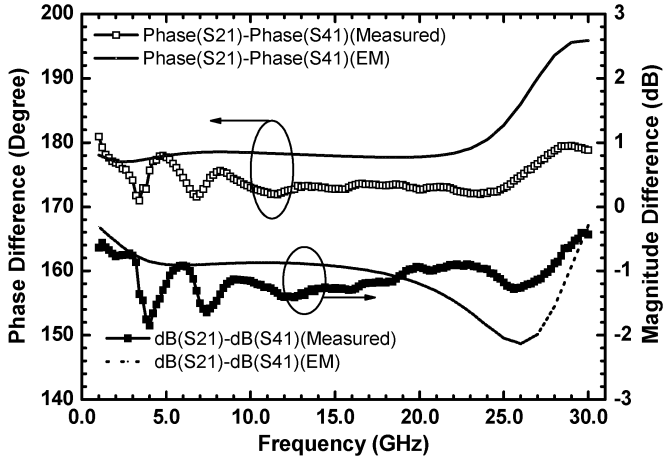


Fig. 11. Phase difference between $S_{21}$ and $S_{41}$ of the rat-race coupler with a phase inverter.

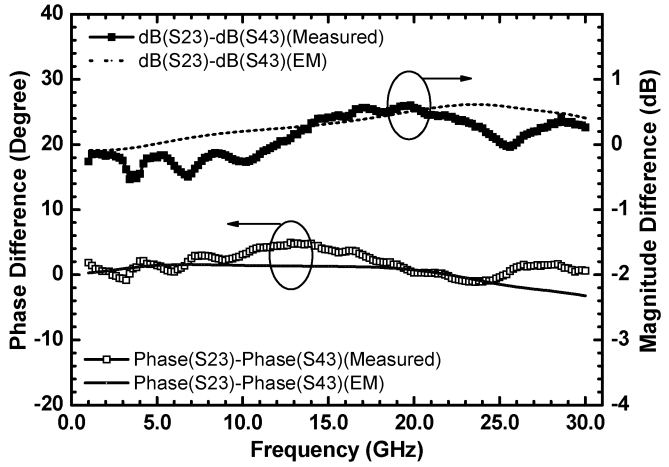


Fig. 12. Phase difference between $S_{23}$ and $S_{43}$ of the symmetrical spiral-shaped rat-race with a phase inverter.

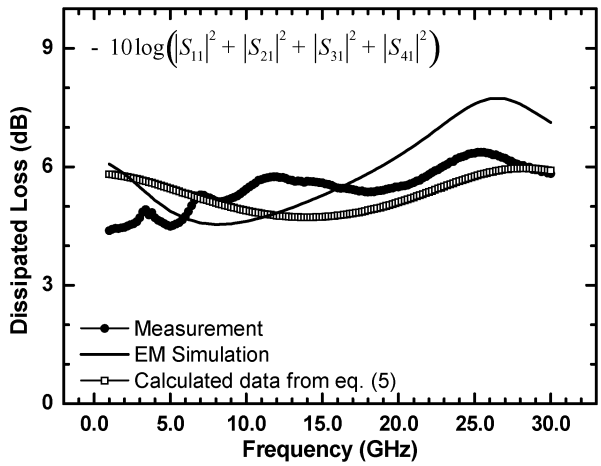


Fig. 13. Dissipated loss of the symmetrical spiral-shaped rat-race with a phase inverter.

A two-port transformer has a broad frequency operation and a low loss. Generally speaking, the upper operation frequency of a two-port transformer is limited by the parasitic capacitances. However, when the transformer is employed as a three-

TABLE I
COMPARISONS OF SILICON-BASED RAT-RACE COUPLERS WITH A PHASE INVERTER

| Ref | Operation Frequency (GHz) | Size ($um^2$) | Method | Through (dB) | Coupled (dB) | Return Loss (dB) | Isolation (dB) | Phase Difference (degree) |
|---|---|---|---|---|---|---|---|---|
| [17] | 25~35 (33%) | 282x314 | Multilayer design with ground plane | -3.1~ -3.18 | -5.1~-5.7 | <-10 | <-17 | 150~200* |
| [19] | 48~80 (50%) | 334x334 | Finite-ground coplanar waveguide (FGCPW) | -4.1~-5 | -5.7~-6.5 | <-10 | <-18.5 | 182~186 |
| | 62~90** | 320x320 | | -4.2~-5 | -5.6~-6.5 | <-10 | <-21 | 184~186.5 |
| This Work | 5~23 (128%) | 707x707 | Spiral-shaped coplanar striplines | -7.96~-9.65 | -9.14~-10.57 | <-10 | <-25 | 171.5~178 |

*From the plot of measured phase difference.

**The upper frequency is limited by the measurement.

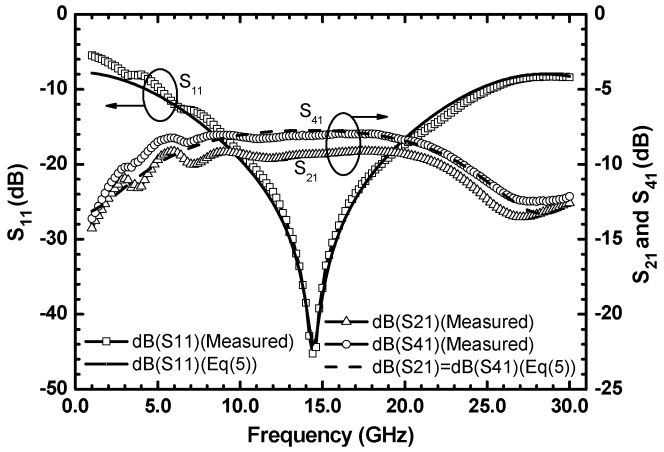


Fig. 14. Calculated $S$-parameters of the rat-race coupler with a phase inverter.

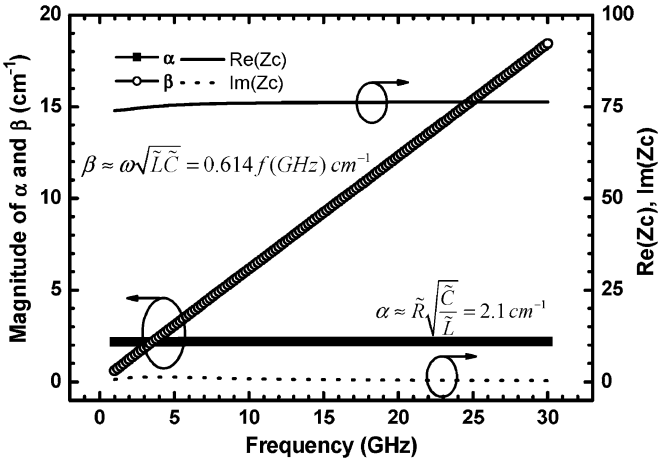


Fig. 15. Calculated characteristic impedance and complex propagation constant of the rat-race coupler with a phase inverter.

port balun, output signal balance at high frequencies is drastically deteriorated since the single-end input signal destroys the transformer's symmetry in EM characteristics [26]. Thus, a three-port transformer balun has much less bandwidth than a two-port transformer has. An active balun is plagued by the dc-power consumption, dynamic range, and noise, in spite of its small size. Therefore, this phase-inverter rat-race coupler is a good choice for a wideband balun.

The comparison results, based on the same return-loss performance ($< -10$ dB), are shown in Table I. Silicon-based phase-inverter rat-race couplers are also implemented with lossless multilayer microstrips [17] and lossy FGCPWs [19]. The lossy couplers in this study and [19] have broader input matching than the lossless counterpart in [17] because of the degradation of the quality factor of the transmission line. The signal balance in our study is better than that of [17] because of the symmetrical design in our phase inverter. When compared with [19], our signal-balance performance is as good as that of the FGCPW coupler, but the fractional bandwidth of our coupler is better because of the lower quality factor of the transmission line when operated at lower frequencies.

### C. Distortionless Transmission Line

By the extraction from the measured four-port $S$-parameters with curve fitting, the values of $\widetilde{R}$, $\widetilde{L}$, $\widetilde{G}$, and $\widetilde{C}$ are

$$\begin{cases} \widetilde{R} = 161\ \Omega/\text{cm} \\ \widetilde{L} = 7.47\ \text{nH/cm} \\ \widetilde{G} = 0.03\ \text{S/cm} \\ \widetilde{C} = 1.28\ \text{pF/cm} \end{cases} \tag{9}$$

and they are close to the values directly extracted from the simulated two-port $S$-parameters of a quarter-wavelength CPS [24]. $S_{11}$ and $S_{21}$, calculated by (5), are plotted in Fig. 14 in comparison with the measurement results. Notice that the ratio of $\widetilde{R}$ to $\widetilde{L}$ ($\widetilde{R}/\widetilde{L} = 21.6\ G\Omega$/H) is close to the ratio of $\widetilde{G}$ to $\widetilde{C}$ ($\widetilde{G}/\widetilde{C} = 23.1$ GS/F). Thus, the lossy transmission line is close to a distortionless transmission line [23]. Thus, the characteristic impedance is almost a real number. As mentioned in Section II, perfect port matching can be achieved at the center frequency of approximately 14.5 GHz. Fig. 15 shows the characteristic impedance and the complex propagation constant, based on the formulas

$$Z_C = \sqrt{\frac{\widetilde{R} + j\omega\widetilde{L}}{\widetilde{G} + j\omega\widetilde{C}}} = \sqrt{\frac{\widetilde{L}}{\widetilde{C}}} \tag{10}$$

and

$$\gamma = \alpha + j\beta = \sqrt{(\widetilde{R} + j\omega\widetilde{L})(\widetilde{G} + j\omega\widetilde{C})} = \frac{\widetilde{R}}{\sqrt{\frac{\widetilde{L}}{\widetilde{C}}}} + j\omega\sqrt{\widetilde{L}\widetilde{C}} \tag{11}$$

where

$$\frac{\widetilde{R}}{\widetilde{L}} = \frac{\widetilde{G}}{\widetilde{C}} \tag{12}$$

for a distortionless transmission line. The characteristic impedance is approximately $76 + 0.6j\ \Omega$ and it fits the

matching equation (6). Moreover, the attenuation constant $\alpha$ is unchanged and the propagation constant $\beta$ is almost a linear function of frequency. Therefore, the coupler is nondispersive. The attenuation of the 1800-$\mu$m distortionless line is approximately 3.28 dB.

## IV. Conclusion

In this paper, the lossy rat-race coupler implemented on the standard silicon substrate has been analyzed and designed. A phase inverter is utilized in this coupler to extend the operation bandwidth and to provide balanced outputs even for the lossy silicon substrate. The transmission lines in the coupler are formed by symmetrical spiral-shaped CPSs to shrink the coupler size, and are designed as a distortionless line for the port matching of the coupler. It is easy to construct a phase inverter in the middle of the symmetrical spiral-shaped CPS. The demonstrated monolithic rat-race coupler, with the size of 0.5 mm$^2$, operates from 5 to 23 GHz, and keeps the output broadband balanced. In addition, a single-ended broadband Gilbert micromixer, along with an LO phase-inverter rat-race coupler, is demonstrated. The mixer functions from 2.5 to 13 GHz and has the conversion gain of 12 dB, $\mathrm{IP}_{1\,\mathrm{dB}}$ of $-16$ dBm, $\mathrm{IIP}_3$ of $-4$ dBm, and noise figure of 14 dB.

## Appendix A
## Derivation of $S_{21} = -S_{41}$

The complex scattering parameters of the coupler are written in (5). Under the condition of $l_a = 2l_b = l$, $\hat{z}_a = \hat{z}_b = \hat{z}$, and $\gamma_a = \gamma_b = \gamma$, the numerator of $S_{21}$ is simplified to

$$\begin{aligned}
&\frac{\hat{z}_a}{\hat{z}_b}\sinh(\gamma_a l_a)\left[\tanh(\gamma_b l_b) - \coth(\gamma_b l_b)\right] \\
&\quad = \sinh(\gamma l)\left[\tanh\left(\frac{\gamma l}{2}\right) - \coth\left(\frac{\gamma l}{2}\right)\right] \\
&\quad = \sinh(\gamma l)\left[\frac{\sinh^2\left(\frac{\gamma l}{2}\right) - \cosh^2\left(\frac{\gamma l}{2}\right)}{\sinh\left(\frac{\gamma l}{2}\right)\cosh\left(\frac{\gamma l}{2}\right)}\right] \\
&\quad = \sinh(\gamma l)\left[-2\,\mathrm{csch}(\gamma l)\right] \\
&\quad = -2
\end{aligned} \tag{A1}$$

where

$$\sinh^2\left(\frac{\gamma l}{2}\right) - \cosh^2\left(\frac{\gamma l}{2}\right) = -1 \tag{A2}$$

and

$$\sinh\left(\frac{\gamma l}{2}\right)\cosh\left(\frac{\gamma l}{2}\right) = \frac{1}{2}\sinh(\gamma l). \tag{A3}$$

Therefore, $S_{21}$ is equal to $-S_{41}$.

## Appendix B
## Derivation of the Normalized Characteristic Impedance and $S_{21}$ of the CPSs for the Perfect Port-Matching

At the center frequency, the numerator of $S_{11}$ can be derived in terms of $l_a = 2l_b = l = \lambda/4$, $\hat{z}_a = \hat{z}_b = \hat{z}$, and $\gamma_a = \gamma_b = \gamma$ as follows:

$$\begin{aligned}
&\sinh(\gamma_a l_a)\left(\hat{z}_a - \frac{1}{\hat{z}_a} - \frac{\hat{z}_a}{\hat{z}_b^2}\right) \\
&\quad - \frac{1}{\hat{z}_b}\cosh(\gamma_a l_a)\left[\tanh(\gamma_b l_b) + \coth(\gamma_b l_b)\right] \\
&\quad = j\cosh\left(\frac{\lambda}{4}\alpha\right)\left(\hat{z} - \frac{2}{\hat{z}}\right) - j\frac{2}{\hat{z}}\sinh\left(\frac{\lambda}{4}\alpha\right)\tanh\left(\frac{\lambda}{4}\alpha\right) \\
&\quad = j\frac{\hat{z}^2\cosh^2\left(\frac{\lambda}{4}\alpha\right) - 2\left[\cosh^2\left(\frac{\lambda}{4}\alpha\right) + \sinh^2\left(\frac{\lambda}{4}\alpha\right)\right]}{\hat{z}\cosh\left(\frac{\lambda}{4}\alpha\right)} \\
&\quad = \frac{j}{\hat{z}\cosh\left(\frac{\lambda}{4}\alpha\right)}\left\{\hat{z}^2\cosh^2\left(\frac{\lambda}{4}\alpha\right) - 2\cosh\left(\frac{\lambda}{2}\alpha\right)\right\}
\end{aligned} \tag{B1}$$

where

$$\begin{cases}
\sinh\left(\frac{\lambda}{4}\gamma\right) = \sinh\left(\frac{\lambda}{4}\alpha + j\frac{\pi}{2}\right) = j\cosh\left(\frac{\lambda}{4}\alpha\right) \\
\cosh\left(\frac{\lambda}{4}\gamma\right) = \cosh\left(\frac{\lambda}{4}\alpha + j\frac{\pi}{2}\right) = j\sinh\left(\frac{\lambda}{4}\alpha\right) \\
\tanh\left(\frac{\lambda}{8}\gamma\right) + \coth\left(\frac{\lambda}{8}\gamma\right) = 2\tanh\left(\frac{\lambda}{4}\alpha\right) \\
\cosh^2\left(\frac{\lambda}{4}\alpha\right) + \sinh^2\left(\frac{\lambda}{4}\alpha\right) = \cosh\left(\frac{\lambda}{2}\alpha\right).
\end{cases} \tag{B2}$$

When

$$\hat{z} = \frac{\sqrt{2\cosh(\lambda\alpha/2)}}{\cosh(\lambda\alpha/4)} \tag{B3}$$

this numerator is equal to zero and the port matching of the coupler is achieved at the center frequency. Under the matching condition, $S_{21}$ at the center frequency can be obtained as

$$\begin{aligned}
S_{21} &= -\frac{2}{D} \\
&= -20\log\left(2\sinh\left(\frac{\lambda\alpha}{4}\right) + \sqrt{2\cosh\left(\frac{\lambda\alpha}{2}\right)}\right)\,(\mathrm{dB})
\end{aligned} \tag{B4}$$

where

$$
\begin{aligned}
D &= 2\cosh(\gamma_a l_a) + 1/\hat{z}_b\left[\hat{z}_a \sinh(\gamma_a l_a) + \cosh(\gamma_a l_a)\right] \\
&\quad \times \left[\tanh(\gamma_b l_b) + \coth(\gamma_b l_b)\right] \\
&\quad + \sinh(\gamma_a l_a)\left(\hat{z}_a + 1/\hat{z}_a + \hat{z}_a/\hat{z}_b^2\right) \\
&= j2\sinh\left(\frac{\alpha\lambda}{4}\right) + 1/\hat{z}\left[\hat{z}j\cosh\left(\frac{\alpha\lambda}{4}\right) + j\sinh\left(\frac{\alpha\lambda}{4}\right)\right] \\
&\quad \times \left[2\tanh\left(\frac{\alpha\lambda}{4}\right)\right] + j\cosh\left(\frac{\alpha\lambda}{4}\right)(\hat{z} + 2/\hat{z}) \\
&= j4\sinh\left(\frac{\alpha\lambda}{4}\right) + \frac{j2\sinh^2\left(\frac{\alpha\lambda}{4}\right) + j2\cosh^2\left(\frac{\alpha\lambda}{4}\right)}{\sqrt{2\cosh\left(\frac{\alpha\lambda}{2}\right)}} \\
&\quad + j\sqrt{2\cosh\left(\frac{\alpha\lambda}{2}\right)} \\
&= j4\sinh\left(\frac{\alpha\lambda}{4}\right) + j2\sqrt{2\cosh\left(\frac{\alpha\lambda}{2}\right)}. \qquad \text{(B5)}
\end{aligned}
$$

## REFERENCES


[1] C. H. Doan, S. Emami, A. M. Niknejad, and R. W. Brodersen, "Millimeter-wave CMOS design," *IEEE J. Solid-State Circuits*, vol. 40, no. 1, pp. 144–155, Jan. 2005.

[2] J. R. Long, "A low-voltage 5.1–5.8-GHz image-reject downconverter RF IC," *IEEE J. Solid-State Circuits*, vol. 35, no. 9, pp. 1320–1328, Sep. 2000.

[3] K. Masu, K. Okada, and H. Ito, "RF passive components using metal line on Si CMOS," *IEICE Trans. Electron.*, vol. E89-C, no. 6, pp. 681–691, Jun. 2006.

[4] T. S. D. Cheung and J. R. Long, "Shielded passive devices for silicon-based monolithic microwave and millimeter-wave integrated circuits," *IEEE J. Solid-State Circuits*, vol. 41, no. 5, pp. 1183–1200, May 2006.

[5] J. Y.-C. Chang, A. A. Abidi, and M. Gaitan, "Large suspended inductors on silicon and their use in a 2-$\mu$m CMOS RF amplifier," *IEEE Electron Device Lett.*, vol. 14, no. 5, pp. 246–248, May 1993.

[6] J. M. Lopez-Villegas, J. Samitier, C. Cane, P. Losantos, and J. Bausells, "Improvement of the quality factor of RF integrated inductors by layout optimization," *IEEE Trans. Microw. Theory Tech.*, vol. 48, no. 1, pp. 76–83, Jan. 2000.

[7] T. Wang, H.-C. Chen, H.-W. Chiu, Y.-S. Lin, G. W. Huang, and S.-S. Lu, "Micromachined CMOS LNA and VCO by CMOS-compatible ICP deep trench technology," *IEEE Trans. Microw. Theory Tech.*, vol. 54, no. 2, pp. 580–588, Feb. 2006.

[8] Y. J. Yoon, Y. Lu, R. C. Frye, and P. R. Smith, "A silicon monolithic spiral transmission line balun with symmetrical design," *IEEE Electron Device Lett.*, vol. 20, no. 4, pp. 182–184, Apr. 1999.

[9] K. T. Chan, A. Chin, S. P. McAlister, C. Y. Chang, J. Liu, S. C. Chien, D. S. Duh, and W. J. Lin, "Low RF noise and power loss for ion-implanted Si having an improved implantation process," *IEEE Electron Device Lett.*, vol. 24, no. 1, pp. 28–30, Jan. 2003.

[10] K. T. Chan, C. H. Huang, A. Chin, M. F. Li, D.-L. Kwong, S. P. McAlister, D. S. Duh, and W. J. Lin, "Large $Q$-factor improvement for spiral inductors on silicon using proton implantation," *IEEE Microw. Wireless Compon. Lett.*, vol. 13, no. 11, pp. 460–462, Nov. 2003.

[11] C. P. Yue and S. S. Wong, "On-chip spiral inductors with patterned ground shields for Si-based RF ICs," *IEEE J. Solid-State Circuits*, vol. 33, no. 5, pp. 743–752, May 1998.

[12] S. March, "A wideband stripline hybrid ring," *IEEE Trans. Microw. Theory Tech.*, vol. MTT-16, no. 6, p. 361, Jun. 1968.

[13] M.-H. Murgulescu, E. Moisan, P. Legaud, E. Penard, and I. Zaquine, "New wideband, $0.67\lambda g$ circumference 180° hybrid ring coupler," *Electron. Lett.*, vol. 30, no. 4, pp. 299–300, Feb. 1994.

[14] B. R. Heimer, L. Fan, and K. Chang, "Uniplanar hybrid couplers using asymmetrical coplanar striplines," *IEEE Trans. Microw. Theory Tech.*, vol. 45, no. 12, pp. 2234–2240, Dec. 1997.

[15] T. Wang and K. Wu, "Size-reduction and band-broadening design technique of uniplanar hybrid ring coupler using phase inverter for M(H)MIC's," *IEEE Trans. Microw. Theory Tech.*, vol. 47, no. 2, pp. 198–206, Feb. 1999.

[16] C.-Y. Chang and C.-C. Yang, "A novel broadband Chebyshev-response rat-race ring coupler," *IEEE Trans. Microw. Theory Tech.*, vol. 47, no. 4, pp. 455–462, Apr. 1999.

[17] M. K. Chirala and C. Nguyen, "Multilayer design techniques for extremely miniaturized CMOS microwave and millimeter-wave distributed passive circuits," *IEEE Trans. Microw. Theory Tech.*, vol. 54, no. 12, pp. 4218–4224, Dec. 2006.

[18] M.-J. Chiang, H.-S. Wu, and C.-K. C. Tzuang, "Design of synthetic quasi-TEM transmission line for CMOS compact integrated circuit," *IEEE Trans. Microw. Theory Tech.*, vol. 55, no. 12, pp. 2512–2520, Dec. 2006.

[19] M. K. Chirala and B. A. Floyd, "Millimeter-wave Lange and ring hybrid couplers in a silicon technology for $E$-band applications," in *IEEE MTT-S Int. Microw. Symp. Dig.*, San Francisco, CA, Jun. 11–16, 2006, pp. 1547–1550.

[20] H.-Y. Chang, P.-S. Wu, T.-W. Huang, H. Wang, C.-L. Chang, and J. G. J. Chern, "Design and analysis of CMOS broadband compact high linearity modulators for gigabit microwave/millimeter-wave applications," *IEEE Trans. Microw. Theory Tech.*, vol. 54, no. 1, pp. 20–30, Jan. 2006.

[21] J. Reed and G. J. Wheeler, "A method of analysis of symmetrical four-port networks," *IEEE Trans. Microw. Theory Tech.*, vol. MTT-4, no. 4, pp. 246–252, Oct. 1956.

[22] S.-C. Tseng, C. C. Meng, C.-H. Chang, C.-K. Wu, and G.-W. Huang, "Monolithic broadband Gilbert micromixer with an integrated Marchand balun using standard silicon IC process," *IEEE Trans. Microw. Theory Tech.*, vol. 54, no. 12, pp. 4362–4371, Dec. 2006.

[23] D. K. Cheng, *Field and Wave Electromagnetics*, 2nd ed. Reading, MA: Addison-Wesley, 1989, pp. 437–444.

[24] Y. Eo and W. R. Eisenstadt, "High-speed VLSI interconnect modeling based on $S$-parameter measurements," *IEEE Trans. Compon., Hybrids, Manuf. Technol.*, vol. 16, no. 5, pp. 555–562, Aug. 1993.

[25] B. Gilbert, "The MICROMIXER: A highly linear variant of the Gilbert mixer using a bisymmetric class-AB input stage," *IEEE J. Solid-State Circuits*, vol. 32, no. 9, pp. 1412–1423, Sep. 1997.

[26] K. Ma, J.-G. Ma, L. Jia, B. Ong, M. A. Do, and K. S. Yeo, "800 MHz $\sim$2.5 GHz miniaturized multi-layer symmetrical stacked baluns for silicon based RF ICs," in *IEEE MTT-S Int. Microw. Symp. Dig.*, Long Beach, CA, Jun. 2005, pp. 283–286.



**Sheng-Che Tseng** (S'05) received the B.S. degree in communication engineering from National Chiao Tung University, Hsinchu, Taiwan, R.O.C., in 2003, and is currently working toward the Ph.D. degree in communication engineering at National Chiao Tung University.

His current research focuses on RF integrated circuits (RFICs) and high-frequency circuitry.



**Chinchun Meng** (M'02) received the B.S. degree in electrical engineering from National Taiwan University, Taipei, Taiwan, R.O.C., in 1985, and the Ph.D. degree in electrical engineering from the University of California at Los Angeles, in 1992.

He is currently a Full Professor with the Department of Communication Engineering, National Chiao Tung University, Hsinchu, Taiwan, R.O.C. His current research interests are in the areas of RFICs and microwave and millimeter-wave ICs.

**Chia-Hung Chang** was born in Taipei, Taiwan, R.O.C., in 1982. He received the B.S. degree in electrical engineering from Yuan Ze University, Taiwan, R.O.C., in 2004, and the M.S. degree in communication engineering from National Chiao Tung University, Hsinchu, Taiwan, R.O.C., in 2006.

He was involved with pseudomorphic HEMT (pHEMT) monolithic microwave integrated circuit (MMIC) amplifiers and SiGe RF mixers during his master's research.

**Shih-Hsien Chang** was born in Kaohsiung, Taiwan, R.O.C., in March 1972. He received the B.S. degree in communication engineering from National Chiao Tung University, Hsinchu, Taiwan, R.O.C., in 1995, and is currently working toward the M.S. degree in communication engineering from National Chiao Tung University.

In 2000, he was with the ISSC Corporation, Hsinchu, Taiwan, R.O.C., where he involved in hardware design for communication systems such as cable modems, wireless local area networks (LANs), and Bluetooth technology. He is currently with Sunplus Technology, Hsinchu, Taiwan, R.O.C., where he develops digital video broadcasting–terrestrial (DVB-T) and advanced television systems committee (ATSC) systems. His research interests include RF/microwave circuits, MMICs, and wireless communication subsystems.

**Guo-Wei Huang** was born in Taipei, Taiwan, R.O.C., in 1969. He received the B.S. degree in electronics engineering and Ph.D. degree from National Chiao Tung University, Hsinchu, Taiwan, R.O.C., in 1991 and 1997, respectively.

In 1997, he joined National Nano Device Laboratories, Hsinchu, Taiwan, R.O.C., where he is currently a Researcher. His current research interests focus on microwave device design, characterization, and modeling.